Case 3.4 Periodic Hills $Re = 10,595$

Laslo T. Diosady * Scott M. Murman †

NASA Ames Research Center, Moffett Field, CA, USA

Code Description

This work uses a higher-order discontinuous-Galerkin finite-element method to solve the compressible Navier-Stokes equations [1,2]. The unsteady Navier-Stokes equations are discretized using a non-linearly stable space-time entropy-variable formulation. The inviscid flux is computed using the approximate Riemann solver of Ismail and Roe [3]. The viscous fluxes are computed using an interior penalty (IP) method equivalent to the second form of Bassi and Rebay (BR2) [4]. Evaluation of the integrals appearing in the DG formulation are performed using a dealiased quadrature rule using $2N$ points in each direction where N is the solution order (in either space or time). The nonlinear problem arising at each time-slab is solved using a Jacobian-free Newton-Krylov method using a diagonalized-ADI preconditioner [5]. Results are presented using the space-time formulation with accuracy up to 16th order ($N = 16$) in both space and time.

The code is parallelized using the Message Passing Interface (MPI). The computations presented in this work are performed using the Sandy Bridge nodes of the NASA Pleiades supercomputer at NASA Ames Research Center. Each Sandy Bridge node consists of 2 eight-core Intel Xeon E5-2670 processors with a clock speed of 2.6Ghz and 2GB per core memory. On a Sandy Bridge node the Tau Benchmark [6] runs in a time of 7.6s.

Case 3.4: DNS of flow over 2D periodic hill

The 2D periodic hill problem has been widely studied as a model problem for separated turbulent flow [7–10]. The geometry consists of a periodic channel with a 2D hill restriction. The size of the domain is $9h \times 3.035h \times 4.5h$ in the stream-wise, wall-normal and span-wise directions, where h is the height of the hill. The flow is driven by a constant body force to ensure a given mass flux.

We consider the flow at a Reynolds number $Re = 10,595$, where the Reynolds number is defined using the bulk velocity and the height of the channel above the hill. Figure 1 shows the mean velocity profile, $\bar{u}$, and the r.m.s. velocity, $u_{rms} = (\overline{u'u'})^{1/2}$ at $Re = 10,595$.

Meshes

Simulations were performed at $Re = 10,595$ using our space-time DG formulation with a 4th-order temporal discretization and an 8th-order spatial discretization. We have used a sequence of meshes using $128 \times 64 \times 64$, $192 \times 96 \times 96$, $256 \times 128 \times 128$ and $384 \times 192 \times 192$ degrees of freedom in stream-wise, wall-normal and span-wise directions. At each mesh resolution 8th-order polynomial curvilinear meshes were generated to match the solution order by defining the location of the Gauss-Legendre-Lobatto nodes for each element using a pseudo-spectral rational interpolation from an underlying structured mesh. The cross-section of the mesh consisting of $16 \times 8 \times 8$ elements, corresponding to the simulation using $128 \times 64 \times 64$ DOFs, is plotted in Figure 1.

*laslo.diosady@nasa.gov
†scott.m.murman@nasa.gov

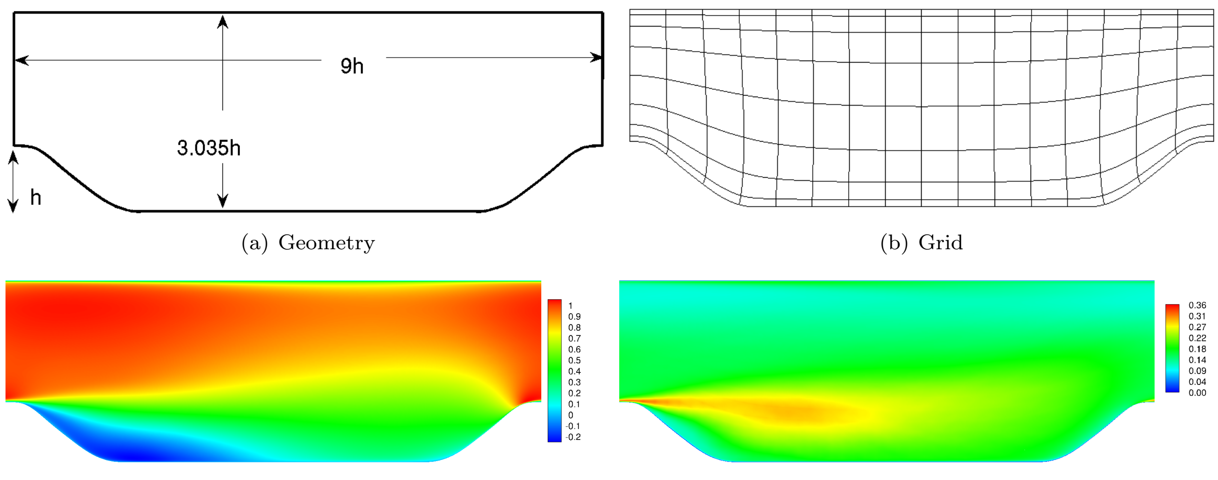

(a) Geometry (b) Grid

(c) $\bar{u}$ (d) u_{rms}

Figure 1: Geometry, Grid, Mean stream-wise velocity, $\bar{u}$ and r.m.s. stream-wise velocity, $u_{rms} = (\overline{u'u'})^{1/2}$ for Periodic Hill at $Re = 10,595$.

Results

The mean pressure and wall shear stress on the lower surface of the channel computed on the finest mesh is presented in Figure 2. The mean shear stress profile shows the primary separation point at approximately $x = 0.20$, with reattachment at $x = 4.37$. This matches well with the experimentally results of Rapp et al. [11] who reported a reattachment point at $x = 4.21$. The computed values are also comparable to the values of $x = 0.19$ and $x = 4.69$, respectively, for the separation and reattachment points, computed in LES simulations by Breuer et al [10]. Table gives the mean separation and reattachment points with increasing mesh resolution. The coarse simulations predict a later separation point and earlier reattachment point, under-predicting the size of the separation bubble. With mesh refinement the DG simulation results converge towards the previously reported data. Detailed analysis of the mean shear stress profiles reveals two additional separation points, corresponding to recirculation bubbles at the base of the hill on the wind-ward side and at the peak of the hill. The existence of these two smaller recirculation bubbles is consistent with previous observations by Breuer et al [10].

Mesh	Separation Point	Reattachment Point
$128 \times 64 \times 64$	0.28	3.94
$192 \times 96 \times 96$	0.22	4.13
$256 \times 128 \times 128$	0.21	4.22
$384 \times 192 \times 192$	0.20	4.37
LES (Breuer et al. [10])	0.19	4.69
Experiment (Rapp et al. [11])	-	4.21

We compare our numerical simulations with experimental data of Rapp et al. [11] and LES data of Fröhlich et al. [8] Figure 3 contains the mean velocity and Reynolds stress profiles computed using the finest mesh resolution at stations with $x \approx 0.05, 2.0, 4.0,$ and 6.0. In the present results, we have plotted the profiles corresponding to data along grid lines, as opposed to constant x stations, in order to simplify our post-processing. Figure 3 shows good agreement between the present simulations, the experiments of Rapp et al. and the LES of Fröhlich et al. Some discrepancies between the computed velocity profiles are attributable to a mismatch in the exact location of the plotted data. The small difference in the size of the separation bubble computed in our simulation and that of Fröhlich et al. [8] is evident in the velocity profiles at $x \approx 4$, where the current DNS simulations is able to better match the experimental results. The Reynolds stress profiles obtained with the DG scheme shows good agreement

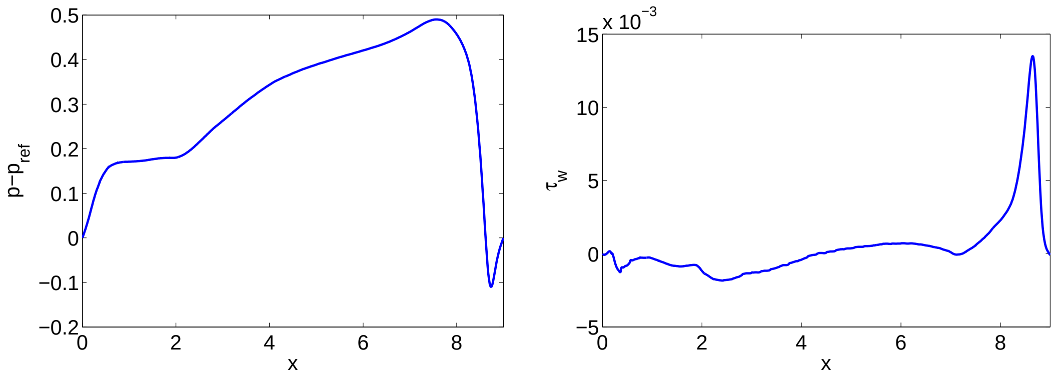

(a) Mean Pressure

(b) Mean Wall Shear Stress

Figure 2: Mean pressure and wall shear stress on lower surface for the periodic hill at $Re = 10{,}595$.

with the reference experimental data and LES data. However, numerical artifacts are apparent in the profiles, which may be due to insufficient statistical convergence. The Reynolds stress profile at $x = 0.05$ shows large values of cross-stream Reynolds stress, $\overline{w'w'}$. This "splatting", corresponding to turbulent kinetic energy being transfered from stream-wise and wall-normal fluctuations to span-wise fluctuations, was previously described by Fröhlich et al. [8]

References

[1] Diosady, L. T. and Murman, S. M., "Design of a variational multiscale method for turbulent compressible flows," AIAA Paper 2013-2870, 2013.

[2] Diosady, L. T. and Murman, S. M., "DNS of flows over periodic hills using a discontinuous Galerkin spectral element method," AIAA Paper 2014-2784, 2014.

[3] Roe, P. L., "Approximate Riemann solvers, parameter vectors, and difference schemes," *Journal of Computational Physics*, Vol. 43, No. 2, 1981, pp. 357–372.

[4] Bassi, F. and Rebay, S., "GMRES discontinuous Galerkin solution of the compressible Navier-Stokes equations," *Discontinuous Galerkin Methods: Theory, Computation and Applications*, edited by K. Cockburn and Shu, Springer, Berlin, 2000, pp. 197–208.

[5] Diosady, L. T. and Murman, S. M., "Tensor-Product Preconditioners for Higher-order Space-Time Discontinuous Galerkin Methods," 2014, under review.

[6] Wang, Z., Fidkowski, K., Abgrall, R., Bassi, F., Caraeni, D., Cary, A., Deconinck, H., Hartmann, R., Hillewaert, K., Huynh, H., Kroll, N., May, G., Persson, P.-O., van Leer, B., and Visbal, M., "High-Order CFD Methods: Current Status and Perspective," *International Journal for Numerical Methods in Fluids*, Vol. 72, 2013, pp. 811–845.

[7] Mellen, C., Frohlich, J., and Rodi, W., "Large-eddy simulation of the flow over periodic hills," *Proceedings of 16th IMACS world congress*, edited by M. Deville and R. Owens, 2000.

[8] Fröhlich, J., Mellen, C. P., Rodi, W., Temmerman, L., and Leschziner, M. A., "Highly resolved large-eddy simulation of separated flow in a channel with streamwise periodic constrictions," *J. Fluid Mech.*, Vol. 526, 2005, pp. 19–66.

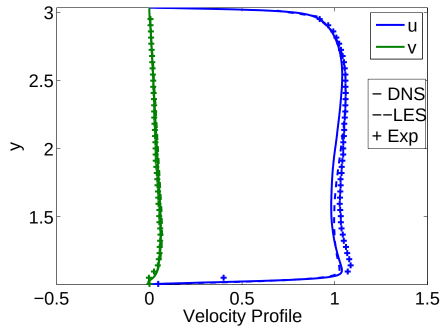

(a) Velocity Profile, $x = 0.05$

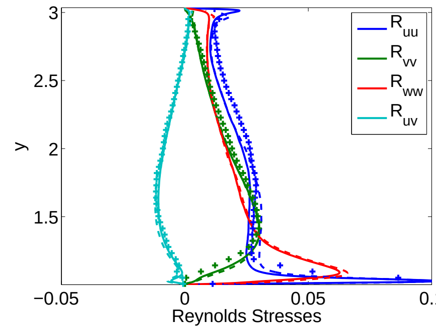

(b) Reynolds Stress, $x = 0.05$

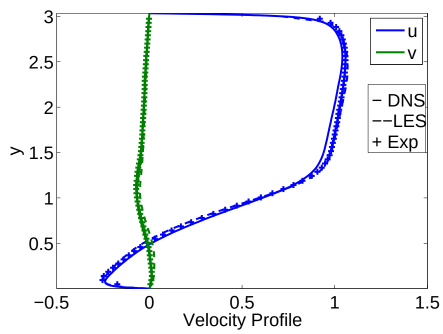

(c) Velocity Profile, $x = 2.0$

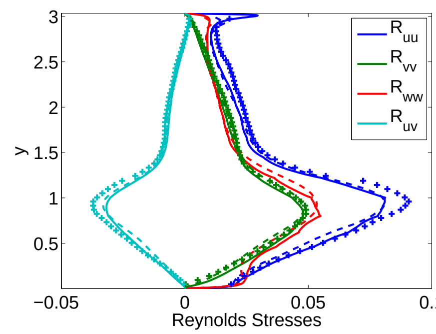

(d) Reynolds Stress, $x = 2.0$

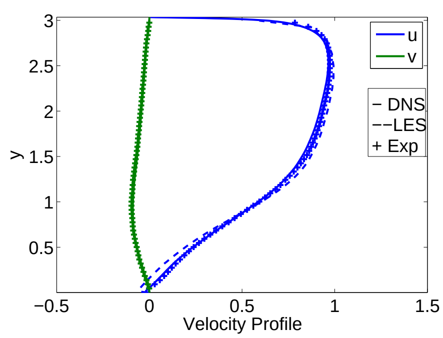

(e) Velocity Profile, $x = 4.0$

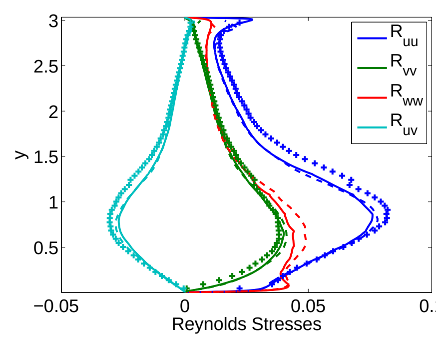

(f) Reynolds Stress, $x = 4.0$

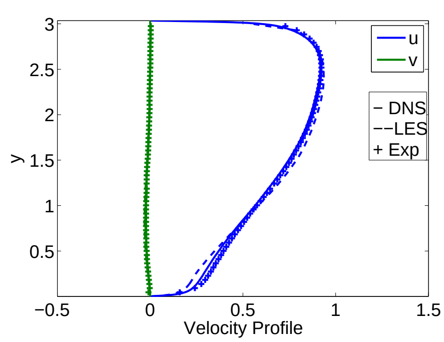

(g) Velocity Profile, $x = 6.0$

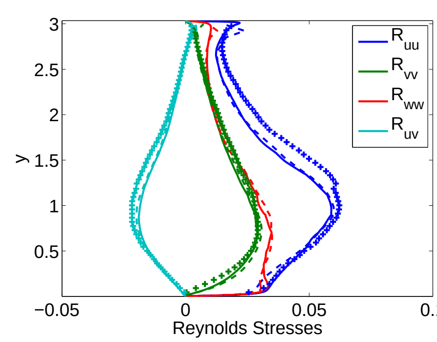

(h) Reynolds Stress, $x = 6.0$

Figure 3: Velocity and Reynolds stress profiles at various stations in the domain for the periodic hill at $Re = 10,595$. (Solid lines are DG solution, dashed lines are LES solution of Fröhlich et al. [8], symbols are experimental results of Rapp et al. [11])

[9] Peller and Manhart, "Turbulent channel flow with periodic hill constrictions," *Arbeitsgemeinschaft Strömung mit Ablösung (STAB)*, edited by Mitteilungen, 2005, pp. 178–179.

[10] Breuer, M., Peller, N., Rapp, C., and Manhart, M., "Flow over periodic hills - Numerical and experimental study in a wide range of Reynolds numbers," *Computers and Fluids*, Vol. 38, 2009, pp. 433–457.

[11] Rapp, C. and Manhart, M., "Flow over periodic hills: an experimental study," *Exp Fluids*, Vol. 51, 2011, pp. 247–269.